Free Volume Model for Transport in Flexible Kerogen of Source Rock's Organic Matter

Kristina Ariskina, Guillaume Galliéro, Amaël Obliger

Free Volume Model for Transport in Flexible Kerogen of Source Rock's Organic Matter

Kristina Ariskina,[†] Guillaume Galliero,[†] and Amaël Obliger[*,‡]

[†]*Laboratoire des Fluides Complexes et leurs Réservoirs, Univ. of Pau and Pays de l'Adour/CNRS/TOTAL/E2S, UMR 5150 Pau 64000, France*

[‡]*Institut des Sciences Moléculaires, Univ. of Bordeaux, CNRS, UMR 5255, Talence 33405, France*

E-mail: amael.obliger@u-bordeaux.fr

Abstract

We build a model of transport of adsorbed fluid within the microprous network of kerogen's microporosity especially accounting for the adsorption induced swelling exhibited by flexible kerogen structures. This model, based on the Fujita-Kishimoto free volume theory that was historically developed for swellable polymers, is built over extensive results for the self-diffusion coefficients obtained by Molecular Dynamics (MD) calculations for a representative molecular model of kerogen designed to study the importance of flexibility effects on the properties of kerogen. To do so, we first highlight that transport within flexible kerogen incorporating the coupling between the dynamics of the fluid molecules and the kerogen matrix atoms does not introduce any significant collective effects in the usual long time limit. Then, we show that despite slightly anisotropic diffusion properties, averaging over all the dimensions can still be performed in order to model the behaviour of the transport properties with the amount of adsorbed fluid while. Last, we link the increase of the self-diffusion coefficients and of the accessible free volume with the fluid loading via the Fujita-Kishimoto model.

We conclude by commenting on the evolution and significance of the model parameters over a broad range of thermophysical conditions.

Introduction

Gas/oil industry has been considerably transformed over the past decades towards exploitation of unconventional reservoirs, such as shales. While the last present huge reserves of hydrocarbons, these resourses are strongly confined in micropores of kerogen, the main phase of the Organic Matter (OM) of shales. Combination of horizontal drilling and hydraulic fracturing[1] partially helps fluids to flow towards exploitation wells by improving the connectivity of the shales' pore space but often at the cost of harming the environment[2,3] and also with strong productivity declines in time that depend non-trivially on the reservoir.[4,5] Possible enhancement of hydrocarbons production from shales with respect for nature requires a deeper knowledge of fluid behaviour in kerogen that remains incomplete.[6]

Unconventional resources — natural gas and oil — generally deposit about 1500 - 4500 meters deep.[7] At these depths kerogen is dispersed in fine grains within clays and rocks.[7,8] Noticeably, kerogen as the oil and gas generator caught the attention of scientists over a century ago.[9] It is currently known that its chemical content and mechanical properties may vary significantly with the depth and kerogen origin that makes it difficult to unify the kerogen properties. Moreover, this OM shows structural heterogenity with predominating meso- and micro-porosity.[10,11] The necessity of accounting kerogen's ultra-confining porosity, amorphous and highly disordered, to describe the transport properties of the adsorbed fluids is challenging.[12–16] Besides, the contribution of chemical/mechanical property of kerogen to the transport properties change during geological (kerogen maturation) or production processes is far from being clear.

A range of fundamental questions on fluid flow within shales have been raised recently.[17–22] Due to the complexity of studying fluid dynamics in kerogen, some insights have been ob-

tained from the couplings between simpler nanoporous structures - carbon based nanoporous materials,[23,24] zeolites[25,26] - and various hydrocarbons. Strong confinement of fluids due to the similarity between the mean free path of fluid molecules and the kerogen pore size has led to the conclusion that transport cannot be described by hydrodynamics.[27] Also, phenomena occuring because of the solid-fluid interactions, such as fluid-slippage, wettability and Knudsen diffusion, have been recognized to have great significance at larger scales than the kerogen's microporosity.[28–39]

Thanks to Molecular Dynamics (MD) calculations and the development of molecular reconstructions of kerogens' microporosity[40–44] it became possible to extensively study fluid-solid couplings by considering the carbon-based matrix. For realistic molecular reconstructions of kerogens' microporosity fluid transport has been determined as diffusive[27,45–47] as fluid-fluid cross-correlations vanish due to the predominance of adsorption effects. As a consequence, attempts to apply conventional laws, such as Darcy's law, describing fluid flow at macroscale have proven unsuccessful. However, some models have been used to rationalize the systematic decrease of the self-diffusion coefficient with the amount of adsorbed fluid.[27,45–47] A linear correlation between the diffusion coefficient and the limiting pore diameter of the microstructure has been highlighted in.[48] In contrast, the matrix flexibility has not been taken into account until very recently,[44,49–51] while coals and immature kerogens that exhibit adsorption induced swelling constitute a significant part of the diversity of source rocks' organic matter.[7] When the microporous matrix is treated as rigid or arbitrarily constrained by "virtual nails",[52] possible deformations are neglected while they can induce important swelling of the microstructure as exemplified in.[44] Noticeably, adsorption induced swelling increase the transport properties as shown previously[50] and illustrated on Fig. 1. While the diffusive nature of fluid transport has been proven for rigid confinement, promoting internal fluid correlations via the matrix's flexibility can lead to collective effects that have not been investigated yet for the case of important adsorption induced swelling.

In the following, after presenting the numerical model for the kerogen microstructure and

the methods used here we start by showing that those collective effects do not arise even in the case of important swellling while fully accounting for the solid-fluid couplings during MD calculations. Then, we highlight that transport in these conditions can be slighthly anisotropic, as noticed for other molecular models,[53,54] while not altering the behaviour of the diffusion coefficient with the amount of adsorbed fluid under adsorption induced swelling. We then correlate the increase of pore volume upon adsorption with the increase of the transport properties for a large diversity of thermophysical conditions by the use of a model based on the Fujita Kishimoto free volume theory developed originally to describe the enhancement of gas mobility in swellable polymers.[55,56] Finally, we analyse the trend of the free volume parameters needed to reproduce the trends of the transport properties with the fluid loading as function of the temperature and the mechanical pressure applied to the systems.

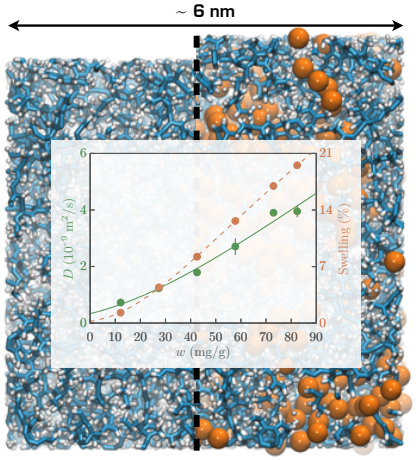

Figure 1: Evolution of the self-diffusion coefficient (green) and the volumetric swelling (red) with the fluid loading w, in mg of fluid per gram of matrix, of adsorbed methane for a temperature of 400 K and a mechanical pressure of 25 MPa within the flexible model of kerogen shown in the background. Its left part represents the matrix with no fluid adsorbed while its right part the swollen system at the highest fluid loading considered (w = 82.4 mg/g). Carbon and hydrogen atoms of the matrix (black and white, resp.) and their covalent bonds are depicted using a ball and stick representation while methane molecules are represented by larger orange spheres. The total volumes of the systems shown are 190 and 228 nm^3, respectively. Visualizations of the free volume distribution are provided in the S.I.

Methods

Kerogen molecular models

The molecular model of type II (immature) kerogen matrix used in the present paper (shown in Fig. 1) has been developed in[44] and allows the study of the poroelastic couplings between the kerogens' microporous structure and the adsorbed fluids that has been shown to be crusial for diffusion.[50] We defer the interested reader to[44] for the numerical procedure of construction of the molecular model and recall here the main features of the kerogen model. The molecular model counts a total of 16864 atoms with an H/C ratio of 1.1 corresponding to a type II kerogen. For the sake of simplicity, the structure is only composed of carbon and hydrogen as it is believed that heteroelements entering the natural composition of kerogens like oxygen, sulfur and nitrogen in lower concentrations have a negligible impact on mechanical properties. A closer inspection of the chemical structure of the molecular model reveals that its texture is mainly composed of short aliphatic chains, containing 5 C atoms on average, and small aromatic ring clusters, containing 10 C atoms on average, with a balanced ring/chain ratio of 0.7. This leads to a "semi-flexible" matrix because of the inclusions of elements contributing to the stiffening (ring clusters) and to the softening (aliphatic chains) of the structure. Consequently, its bulk modulus is moderate ($\simeq$ 1-5 GPa) and consistent with type II immature kerogens. For geological conditions, the bulk modulus of the matrix decreases with the decrease of the pressure P, the increase of the temperature T and the fluid loading w expressed in mg of fluid per g of matrix. We emphasize here that the mechanical pressure applied to the system does not correspond to any bulk fluid pressure but to the lithostatic pressure. In shales, the *mechanical* pressure is imposed by geology and the fluid loading depends on the geological history: i. e. how many hydrocarbons were produced upon maturation and how much of them were expelled. Thus, as in,[44] we treat the pressure and the fluid loading as independent variables.

Moreover, as the matrix and fluid only consist in carbon and hydrogen atoms, the de-

scription of inter- and intra-molecular interactions during Molecular Dynamics (MD) simulations is carried by the the modified adaptive intermolecular reactive empirical bond order (AIREBO) potential.[44] The AIREBO potential has proved to be highly realsitic to describe a large number of carbon-containing molecular models. The long range part of the AIREBO potential has been slightly modified in[44] so as to reproduce more accurately the equation of states of linear alkanes. This reparameterization was motivated by the fact that the density of the kerogen structure is the key quantity controling the properties of the molecular structure.

Fluid diffusion within flexible kerogen has been investigated in [50] for this molecular model, emphasizing on the importance of the adsorption induced swelling phenomenon, but only for a few thermodynamical conditions, and for a few nanoseconds thus limiting the study to the self-diffusion coefficients. This limitation was caused by the use of a homemade MD code with a correct implementation of the AIREBO potential as opposed to its initial implementation in the LAMMPS package. This has been corrected by[57] proposing a vectorized and parallelized implementation of AIREBO that is particularly efficient.

We take advantage of these performances to explore a larger diversity of thermo-mechanical conditions (temperature, pressure) and longer simulations times to obtain accurate estimations of the self-diffusion coefficients and even investigate collective diffusion coefficients that could not be investigated before. Besides the typical geological T/p, temperature and pressure above (500 K and 100 MPa, correspondingly) and below (300 K and 0.1 MPa, correspondingly) this condition were considered. The number of adsorbed fluid molecules considered varies from 80 to 542 with the following fluid loadings expressed in milligrams of fluid per gram of kerogen: 12.1 (80), 27.3 (180), 42.5 (280), 57.7 (380), 72.9 (480) and 82.4 (542). According to the increase of fluid amount, volumetric characteristics, such as the porosity (volume fraction not occupied by the matrix atoms), free volume (volume fraction not occupied by the matrix and fluid atoms), swelling, also increase in the flexible case. Swelling at the typical geological condition for the lowest methane amount is about 1%,

while for the highest about 20%, volumetric swelling under adsorption is shown in the S.I. for various conditions.

Molecular dynamics setup

In order to generate the trajectories, all-atoms MD calculations of the kerogen model with adsorbed fluid have been performed in the canonical ensemble (NVT) with a timestep of 0.25 fs. The Nosé-Hoover thermostat was used to control the temperature following[58] with a damping parameter of 0.4 ps. Three-dimensional periodic boundary conditions have been applied during the simulations. The constant volumes enforced during the MD trajectories at various conditions (temperature, pressure, loading) come from the results obtained in the isothermal-isobaric ensemble (NPT) and are taken from.[44] Despite rigorously equilibrated volumes it has taken longer trajectories for systems with the lowest fluid quantities. The total time for the lowest (80 molecules) fluid loading therefore have amounted to 50 ns instead of 10 ns for larger fluid loadings.

Pore volume characterization

The pore volume characteristics, the porosity and the free volume ratio, of the kerogen model under different conditions, are computed from equilibrated configurations with methods initially reported in.[44] We briefly recall here the procedures.

The porosity is calculated by considering randomly inserted dimensionless points in the simulation box. The ratio of number of positions that do not get into the C/H atoms of kerogen matrix against the total number of positions is used to obtain the porosity or the free volume ratio if we also discriminate the points lying into the fluid molecules. The atoms are considered as spheres with diameters taken to be their Lennard-Jones parameters taken from the AIREBO potential used in this work: 3.36 and 2.42 Å for carbon and hydrogen atoms, respectively. Fifty thousands random trials are typically needed to reach convergence. The volumetric swelling is simply calculated by comparing the volume of the methane-containing

matrix with the volume of the empty kerogen matrix at the same temperature-pressure conditions.

For the accessible quantities (porosity and free volume ratio), a collection of spheres (2.5 10^5) with a diameter of 3.8 Å, corresponding to the kinetic diameter of methane,[59] that fit into the pore volume is first generated. Then, the accessible porosity is sampled by checking the ratio of random points lying in this collection of spheres. The accessible free volume ratio is estimated by substracting the volume of the adsorbed methane molecules.

Diffusion coefficients calculation

As emphasized recently in[27,45,47] for molecular kerogen structures the steady-state transport properties can be obtained from the collective diffusion coefficient of the adsorbed fluid that can be simply obtained from equilibrium MD calculations. After a sufficiently long time, the Mean Square Displacement (MSD) of a fluid molecule in one of the three dimension within the reference frame of the solid, $\langle \Delta x^2(t) \rangle = \langle (x(t+t_0) - x(t_0))^2 \rangle$ with t the time, reaches a linear regime that allows to evaluate the self diffusion coefficient D_s from

$$\langle \Delta x^2(t) \rangle = 2D_\mathrm{s}\, t + A\,. \tag{1}$$

In practice, for each trajectory, the MSD is averaged over the adsorbed fluid molecules and a sliding average over the initial time t_0 is achieved. Similarly, tracking the MSD of the fluid center of mass (x_c) allows to evaluate the collective diffusion coefficient D_c from

$$\langle \Delta x_\mathrm{c}^2(t) \rangle = 2\frac{D_\mathrm{c}}{N}\, t + B \tag{2}$$

with N the number of fluid molecules. The linear fits used to determine the self- and the collective diffusion coefficients are performed from few hundred ps to 10 ns or 50 ns, respectively. Error bars are estimated from 5 independent trajectories for each condition.

Results

Collective diffusion study

We first investigate the collective effects impacting the long term diffusion process within the flexible kerogen matrix. This is achieved by comparing the collective- and self-diffusion coefficients that differ by cross correlations terms, quantifying those collective effects, as shown by

$$D_{\mathrm{c}} = D_{\mathrm{s}} - \lim_{t\to+\infty} \frac{1}{tN} \sum_{i\neq j} \langle x_i(t) x_j(0) \rangle \,. \tag{3}$$

This expression is obtained by using the definition of the c.o.m. in Eq. 2 and relating Eqs. 1 and 2 in the long time limit. Alternatively, as recalled in[27,44] the Green-Kubo relationship can be invoked to express the cross term in the form of the integral of the velocity cross correlation function as

$$D_{\mathrm{c}} = D_{\mathrm{s}} + \lim_{t\to+\infty} \frac{1}{N} \sum_{i\neq j} \int_0^t \langle v_i(t') v_j(0) \rangle \, \mathrm{d}t' \,. \tag{4}$$

Collective diffusion coefficients are displayed with the self-diffusion coefficients for comparison on Fig. 2 as function of the fluid loading for some thermodynamical conditions - 300/400/500 K and 25 MPa while fully accounting for the viscoelastic nature of the kerogen matrix (swelling and dynamical coupling between fluid and solid atoms). When adsorption induced swelling is important under constant mechanical pressure, the increase of fluid loading is accompanied by an increase in accessible free volume (Fig. 5) that enhances diffusion. We observe that the self-diffusion coefficient and the collective one lie within error bars for each loading at each temperature. It is clear that the trends are the same for both diffusion coefficients at 300 K. At 500 K, it should also be the case since the difference between both coefficients should vanish in the infinite dilution limit. Then, at 400 K, where the trend is unclear, we add that there is no physical reason for the behavior of the collective diffusion

coefficient to be qualitatively different from the two other temperatures. MSD's for the fluid c.o.m. from single trajectories at 400 K are shown in the S.I. We therefore conclude that both coefficients follow the same increasing trends with the fluid loading for the large range of conditions investigated here. This indicates that the cross-correlations between fluid molecules (cross terms in Eqs. 3 and 4) do not significantly contribute to the collective diffusion coefficient. The physical meaning is as follows: diffusion within a flexible kerogen is not affected by long-range hydrodynamic couplings since only individual trajectories' informations captured by the self-diffusion coefficient are needed. It has been recently proven[27,47] that fluid transport is purely diffusive in kerogens' microstructures arbitrarily treated as rigid, thus by neglecting both adsorption induced swelling and the matrix dynamics. The approximation of fully rigid kerogen microporosity may be only relevant for extremely mature kerogens. However, the majority of kerogens exhibits viscoelastic behaviour and, consequently, the molecular models of kerogens' microporosity should be able to deform during MD calculations. Here we show for the first time that, while matrix flexibility plays a significant role on fluid transport, diffusion increases due to adsorption induced swelling as opposed to the rigid behaviour where the shared porous volume remains constant as the fluid loading increases, the impact of the motion of the kerogen matrix do not promote significant cross-correlations between fluid molecules during diffusion within the deformable matrix.

Consequently, no significant collective effects arise on transport properties as for the rigid kerogen approximation. Transport within flexible kerogen matrix can as well be considered purely diffusive despite that pore fluctuations significantly enhance the transport properties.[44] From the computational point of view, there is no need to calculate the collective diffusion coefficient that requires very long trajectories, thus effectively saving computational time since diffusion can be studied by focusing on the self-diffusion properties only.

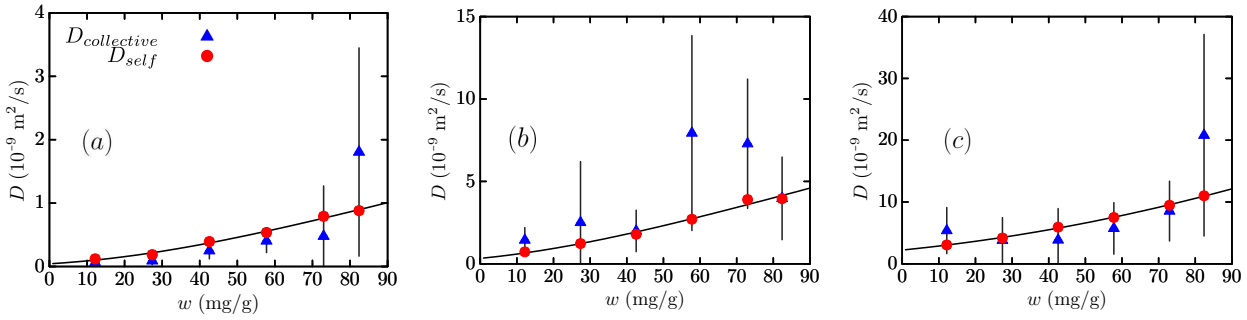

Figure 2: Self- and collective diffusion coefficients of methane as function of the fluid loading for a confinement pressure of 25 MPa and three different temperatures: (a) 300 K, (b) 400 K and (c) 500 K. Larger error bars for the collective diffusion coefficients stems from the fact that only the c.o.m. of the fluid can be tracked from an MD trajectory instead of all the N (ranging from 80 to 542 for the lowest to the highest loading) fluid molecules in the case of the self-diffusion coefficient.

Anisotropy effects

Since performing all-atoms MD calculations for molecular models of kerogen is greatly time consuming the size of the systems studied is limited to a few nanometers. Size effects can arise due to this limitation and since the transport mechanism is locally dominated by the solid-fluid interactions due to the strong adsorption effects we specifically turn our attention to anisotropic effects. We verify here if the molecular model used here with a size of about $6 \times 6 \times 6 \ \ nm^3$ lead to anisotropic transport properties. Figure 3a shows the self-diffusion coefficient over the x, y and z directions for 25 MPa and 400 K (with similar results for other conditions). We note that diffusion along the y direction stands out of diffusion in the two other directions that remains very similar while increasing the fluid loading. In order to quantitatively estimate this trend against the amount of adsorbed fluid molecules, we introduce the anisotropy factor defined as the ratio between the self-diffusion coefficient in the y direction and the averaged self-diffusion coefficient over the two other directions x and z. As can be seen on Fig 3b, the anisotropy factor is approximately constant as function of the fluid loading and remains moderate (<2) without any observable temperature effect. Then, even if the transport properties can differ in one direction, their behaviours with the fluid loading and thus with the adsorption induced swelling are very similar. Since

a small molecular model designed to perform MD calculations cannot reproduce the true heterogeneity of the kerogen's microporous network trapped in a particular hydrocarbon reservoir, averaging the absolute value of slightly anisotropic diffusion coefficients does not represent a problem as long as the trends investigated are not impacted. Consequently, the transport properties of the kerogen matrix, averaged over the three directions, can be considered isotropic. From that, the molecular model of kerogen with a typical size of 6 nm can be used to derive a transport model even if the absolute values of the diffusion coefficients can slightly differ over the directions.

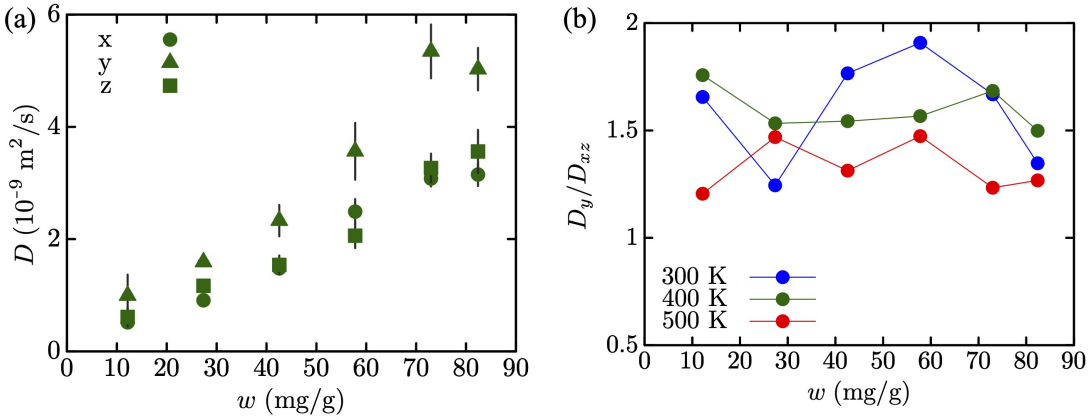

Figure 3: Self-diffusion coefficients along x, y and z directions at 400 K, 25 MPa (a) and anisotropic factor defined as the ratio of the diffusion coefficient in the y direction over the average difusion coefficient in the two other directions (b) as function of the fluid loading for three different temperatures and a pressure of 25 MPa. Similar results are found for other conditions and shown in the S.I..

Free volume model for swellable kerogen

Following recent work on fluid transport accounting matrix flexibility effects,[50] the investigation of the methane self-diffusion coefficient has been performed for a large set of thermodynamical conditions. The prescribed mechanical pressures are 0.1, 25 and 100 MPa for three different temperatures each, 300, 400 and 500 K. As said in the numerical procedure section we benefit from the efficient implementation of the AIREBO force field within the LAMMPS MD calculation package[57] in order to obtain accurate estimations of the self-diffusion coeffi-

cients. This can be seen on Fig. 4 which gathers the evolution of the self-diffusion coefficient with the fluid loading as well as the error bars (95% confidence intervals) estimated from 5 independent runs for the three different confining pressures and temperatures investigated here. Such accuracy notably allows to obtain clear trends for the parameters of the free volume model detailed later.

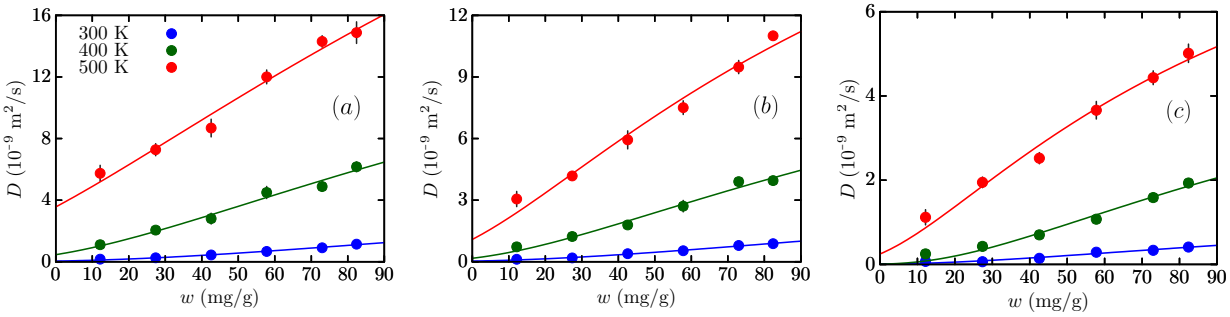

Figure 4: Evolution of the self-diffusion coefficient with the fluid loading for three different temperatures an pressures, (a) 0.1, (b) 25 and (c) 100 MPa. The solid curves correspond to the free volume model with the parameters $\alpha(T,P)$ and $\xi(T,P)$ estimated from a best fit procedure and collected on Fig. 7.

Contrary to the transport properties within a molecular model of kerogen totally frozen, the more there are fluid molecules adsorbed in a flexible kerogen matrix, the greater the diffusion is (Fig. 4). In our case, both the swelling and the coupling between the dynamics of the matrix and the fluid contribute to a faster diffusion compared to the MD studies where the microstructure is held rigid during the simulations.[27,45–47] Alternatively, swelling of the microstructure has been partially accounted for in[52] by freezing some atoms of the structure ("virtual nails") thus restricting the volume increase of the system upon adsorption so much that transport decreases with the gas pressure as in the rigid case. The use of "virtual nails" prevents the microstructure composed of independent molecules to dissolve as shown in.[60] Furthermore, since transport is investigated in a non-equilibrium MD setup with explicit gas reservoirs imposing their pressure to the kerogen model in the longitudinal direction while keeping the dimension of the system fixed in the orthogonal directions during the simulations, unphysical stress and anisotropy within the kerogen structure might arise

and could also explain the diffusion decrease with the gas pressure reported in.[52]

We note that this diffusion increase is more important for larger temperatures and for lower mechanical pressures (notice the different scales on the three different graphs of Fig. 4). The following tendency has been determined within used ranges of thermodynamic parameters: the self-diffusion coefficient increases in about 5.5-9 times more while increasing temperature from 300 to 500 K than decreasing pressure from 100 to 0.1 MPa. Thus, the strongest impact on the diffusion coefficient has the temperature. The pressure affects more the diffusivity than the investigated fluid amount.

This enhancement of the methane transport with the fluid loading results from the matrix swelling under constant applied mechanical pressure and, consequently, the increase of the accessible free volume ratio, φ_{f} which is quantified on fig. 5. In the following we describe its evolution with the fluid loading w as linear,

$$\varphi_{\mathrm{f}}(w) = \varphi_0 + \beta w \tag{5}$$

with φ_0 the accessible proposity with no fluid adsorbed and β a coefficient capturing the increase of free volume under adsorption induced swelling. Their own evolutions with the thermodynamical conditions are summarized on Fig. 6. The negligible temperature variation of φ_0 at the largest pressure investigated (100 MPa) along with the linear evolution of β with the temperature shows that thermal expansion at this pressure develops only when fluid is adsorbed in the matrix. Otherwise, decreasing the mechanical pressure allows for important thermal expansion even at zero loading. Finally, we notice that the coefficient β mostly depends on the temperature and not that much on the pressure.

Because of the strong dependence of the diffusion coefficient on the accessible free volume increase, we propose the Fujita-Kishimoto free volume theory[55,56]

$$D(w) = D_0 \exp\left[\alpha \frac{\varphi_f(w) - \varphi_0}{\varphi_0 \varphi_f(w)}\right] \tag{6}$$

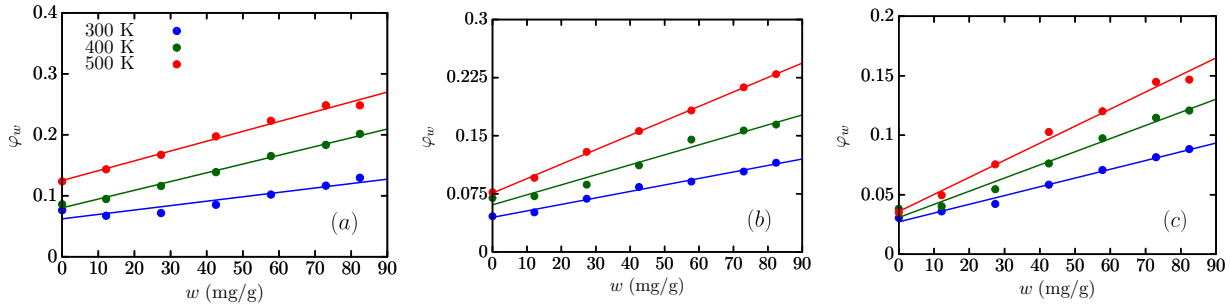

Figure 5: Evolution of the accessible free volume ratio with the fluid loading for the three different tempereatures at (a) 0.1 MPa, (b) 25 MPa, (c) 100 MPa. The solid curves stand for linear fits with the parameters $\varphi_0(T,P)$ and $\beta(T,P)$ estimated from a best fit procedure and gathered on fig. 6.

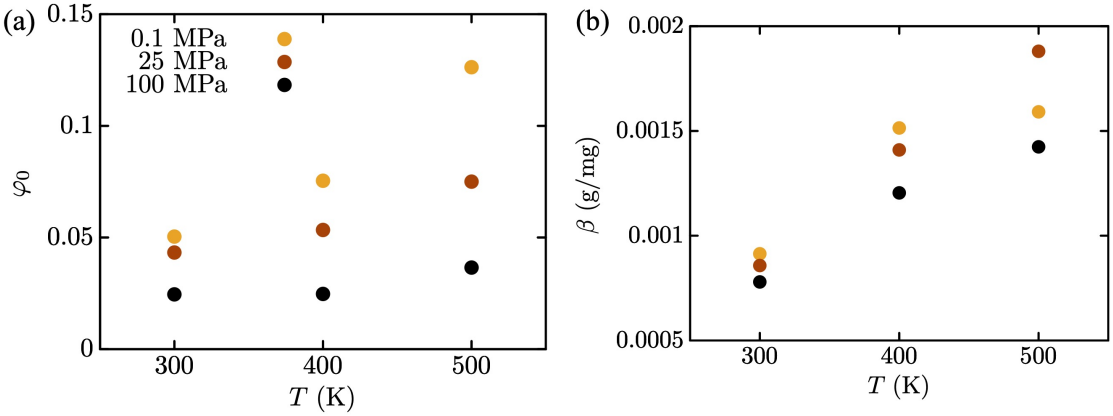

Figure 6: Accessible free volume ratio of the empty matrix φ_0 (a) and linearity coefficient β (b) capturing the increase of the accessible free volume with the fluid adsorption under constant applied mechanical pressure.

to model the transport properties evolution with the fluid loading. We have introduced here the diffusion coefficient in the zero loading limit $D_0 = \frac{k_B T}{\xi_0}$ with ξ_0 the friction coefficient and α the free volume coefficient that reflects on the ability of the fluid molecules to take advantage of the increasing accessible free volume to diffuse faster. In general those parameters depend on the fluid, the matrix and the temperature and pressure. Developing this equation (Eq. 6) with D_0 and the linear expression Eq. 5 for the accessible free volume ratio gives

$$D(w) = \frac{k_B T}{\xi_0} \exp\left[\alpha \frac{\beta w}{\varphi_0(\varphi_0 + \beta w)}\right], \tag{7}$$

a model that can be confronted to the diffusion coefficients displayed on Fig. 4. The parameters α and ξ_0 are fitted against those diffusion coefficients with the parameters related to the free volume evolution, φ_0 and β, imposed and taken from Fig 6. As can be clearly seen on Fig. 4 the resulting model is in very good agreement with the data and can be used to capture the increasing trend of the transport properties with the fluid loading caused by the swelling. The obtained values of the free volume parameters, ξ_0 and α, are reported as function of the temperature and pressure on Fig 7. The friction coefficient ξ_0 decreases with the temperature because of thermal expansion that leads to an increase of the accessible free volume that is also accompanied by a lowering of the local energy barriers in the limit of very low fluid loading. In such conditions, the adsorption induced swelling is critical since the pore space is mostly closed and diffusion is heavily impacted by the local matrix fluctuations.[50] On the contrary, when the swelling is important, the connectivity of the pore space is better and pore size fluctuations become less influential. Globally, the friction coefficient increases with the mechanical pressure for the same physical reasons as increasing the pressure restricts the swelling. We see at large pressure (100 MPa) that the friction does not evolve between 300 and 400 K because the accessible free volume ratio remains constant (Fig. 6a). For the two other pressures, fitting the data with an Arrhenius law leads to energy barriers of 0.23 and 0.17 eV for 0.1 and 25 MPa, respectively. In turn, the free volume coefficient α (Fig. 7b) is relatively unaffected by the thermal expansion. Though, at very low mechanical pressure, 0.1 MPa, the coefficient α is slightly increasing. To check the sensitivity of the model to the parameter α, Fig. 5 of the S.I. shows the adequacy of the model for averaged values of α for each pressure while leaving untouched the values of ξ_0. We see that for the highest pressure (100 MPa) the model becomes very sensitive to α especially for 400K and 500K, while for 25 MPa and 0.1 MPA the model remains accurate. Using a single averaged value for α (see Fig. 6 of the S.I.) gives satisfactory results only for the intermediate pressure of 25 MPa.

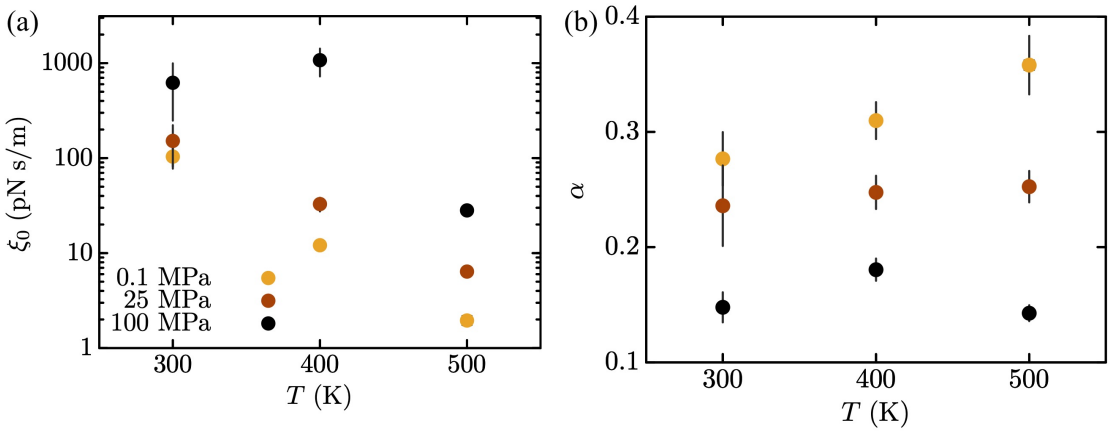

Figure 7: Friction coefficient ξ_0 (a) and the free volume parameter α (b) obtained from a best fit procedure with the parameters ϕ_0 and β corresponding to the different conditions taken from Fig. 6.

Discussion and Conclusions

This study reaffirms clearly that adsorption induced swelling plays a crucial role on transport properties in kerogen microstructures that cannot be considered mechanically rigid. Consequently the transport properties increase with the fluid loading instead of decreasing in the case of kerogen matrices that exhibit no significant volume change upon adsorption. For the first time, it is shown that fluid transport within a flexible kerogen microporous structure is diffusive as it has been previously established within the rigid solid approximation. The matrix flexibility does not promote long-living cross-correlations between fluid molecules and, thus, fluid diffusion properties may be obtained by computing only the self-diffusiion coefficients that can be obtaine at lower computational costs.

The transport properties of the flexible kerogen matrix studied here were found to be slightly anisotropic, in one direction diffusion is less than twice that in the two other directions. Moreover, the analysis of the anisotropic ratio showed that the self-diffusion coefficient trends with the fluid loading over three directions are similar. Consequently, the evolution of the transport properties can be studied by averaging over the three directions for our molecular model with a typical size of 6 nm.

The self-diffusion of methane within a flexible kerogen microstructure was investigated as

function of the fluid loading for a wide range of thermophysical conditions. The systematic increase of the transport properties with the amount of adsorbed fluid due to swelling has been successfully captured by the proposed Fcollectiveujita-Kishimoto free volume model. Once the evolution of the accessible free volume ratio is known, it requires two parameters to describe the diffusion trend with the adsorbed induced swelling. For moderate pressures we show that ξ_0, the friction coefficient in the zero loading limit, declines strongly with the temperature due to the thermal expansion and that its dependence to the pressure at constant temperature is moderate. Also, the free volume coefficient alpha that controls the increasing trend of the transport properties is relatively independent of the temperature and that, again, its dependence on pressure is quite moderate. All of this points in the same direction, the increase of the accessible free volume associated to adsorption induced swelling controls the long-term diffusion process. The parameter α captures the ability of the fluid molecules to use the available free volume to diffuse faster, which incorporates two effects: the possible increase of the available free volume per fluid molecule and the improvement of the pore space connectivity as the matrix swells upon adsorption.

As a final note, the free volume model developed here to rationalize the impact of the kerogen's microstructure flexibility on transport can be used in a multiscale approach to study the transport properties of source rocks' organic matter including pore space and phase heterogeneities at larger scales. Such a task is complicated by the definition of a Representative Elementary Volume (REV) for each phase (and scale) of the multiscale media, as is widely known in the porous media community. For the microporous phase of the kerogen part of source rock's organic matter we are clearly limited in term of size by the cost of the MD calculations for the generation of the molecular model itself (including the equilibration with an adsorbed fluid) and by the long trajectories we need to obtain accurate estimate of the coefficients. In this study, for a molecular model that can allow to study the impact of important swelling, a typical size of 6 nm is enough to obtain a robust model for the transport properties despite low anisotropy. At the mesoscale ($\sim$100 nm) we might be confident that

the transport properties of the microporous phase of kerogen are anisotropic. Our results then suggest that if anisotropies arise within the microporous phase of kerogen, they only have a moderate impact and happen typically at the nanometer length scale. Of course, heterogeneities can be present at the mesoscale such as dispersed mesopores, as revealed by electron microscopy in,[10] or simply by possible variations of the textural and structural properties of the microporous phase over tens of nanometers. Studying these heterogeneities and their impact on transport within the source rocks' organic matter is a challenge we should face in the future.

Supplementary Information

Configuration files for the microporous structure at various conditions investigated in this article can be obtained upon request.

References

(1) Yethiraj, A.; Striolo, A. Fracking: What Can Physical Chemistry Offer? *The Journal of Physical Chemistry Letters* **2013**, *4*, 687–690.

(2) Estrada, J. M.; Bhamidimarri, R. A review of the issues and treatment options for wastewater from shale gas extraction by hydraulic fracturing. *Fuel* **2016**, *182*, 292–303.

(3) Sun, Y.; Wang, D.; Tsang, D. C. W.; Wang, L.; Ok, Y. S.; Feng, Y. A critical review of risks, characteristics, and treatment strategies for potentially toxic elements in wastewater from shale gas extraction. *Environment International* **2019**, *125*, 452–469.

(4) Patzek, T. W.; Male, F.; Marder, M. Gas production in the Barnett Shale obeys a simple scaling theory. *Proceedings of the National Academy of Sciences* **2013**, *110*, 19731–19736.

(5) Cueto-Felgueroso, L.; Juanes, R. Forecasting long-term gas production from shale. *Proceedings of the National Academy of Sciences* **2013**, *110*, 19660–19661.

(6) Striolo, A.; Cole, D. R. Understanding Shale Gas: Recent Progress and Remaining Challenges. *Energy Fuels* **2017**, *31*, 10300–10310.

(7) Vandenbroucke, M.; Largeau, C. Kerogen origin, evolution and structure. *Organic Geochemistry* **2007**, *38*, 719–833.

(8) Gupta, N.; Fathi, E.; Belyadi, F. Effects of nano-pore wall confinements on rarefied gas dynamics in organic rich shale reservoirs. *Fuel* **2018**, *220*, 120–129.

(9) White, W. Some relations in origin between coal and petroleum. *Journal of the Washington Academy of Science* **1915**, *5*, 189–212.

(10) Berthonneau, J.; Obliger, A.; Valdenaire, P.-L.; Grauby, O.; Ferry, D.; Chaudanson, D.; Levitz, P.; Kim, J. J.; Ulm, F.-J.; Pellenq, R. J.-M. Mesoscale structure, mechanics, and transport properties of source rocks' organic pore networks. *Proceedings of the National Academy of Sciences* **2018**, *115*, 12365–12370.

(11) Berthonneau, J.; Grauby, O.; Jolivet, I. C.; Gelin, F.; Chanut, N.; Magnin, Y.; Pellenq, R. J.-M.; Ferry, D. Nanoscale Accessible Porosity as a Key Parameter Depicting the Topological Evolution of Organic Porous Networks. *Langmuir* **2021**, *37*, 5464–5474.

(12) Loucks, R. G.; Reed, R. M.; Ruppel, S. C.; Hammes, U. Spectrum of pore types and networks in mudrocks and a descriptive classification for matrix-related mudrock pores. *AAPG Bulletin* **2012**, *96*, 1071–1098.

(13) Fathi, E.; Akkutlu, I. Y. Lattice Boltzmann Method for Simulation of Shale Gas Transport in Kerogen. *SPE Journal* **2013**, *18*, 27–37.

(14) Fan, D.; Ettehadtavakkol, A. Analytical model of gas transport in heterogeneous hydraulically-fractured organic-rich shale media. *Fuel* **2017**, *207*, 625–640.

(15) Kou, R.; Alafnan, S.; Akkutlu, I. Y. Multi-scale Analysis of Gas Transport Mechanisms in Kerogen. *Transport in Porous Media* **2017**, *116*, 493–519.

(16) Cudjoe, S.; Barati, R. Lattice Boltzmann simulation of CO2 transport in kerogen nanopores—An evaluation of CO2 sequestration in organic-rich shales. *Journal of Earth Science* **2017**, *28*, 926–932.

(17) Freeman, C.; Moridis, G.; Blasingame, T. A Numerical Study of Microscale Flow Behavior in Tight Gas and Shale Gas Reservoir Systems. *Transport in Porous Media* **2011**, *90*, 253–268.

(18) Yethiraj, A.; Striolo, A. Fracking: What Can Physical Chemistry Offer? *The journal of physical chemistry letters* **2013**, *4*, 687–690.

(19) Cole, D. R.; Ok, S.; Striolo, A.; Phan, A. Hydrocarbon Behavior at Nanoscale Interfaces. *Reviews in Mineralogy and Geochemistry* **2013**, *75*, 495–545.

(20) Lee, T.; Bocquet, L.; Coasne, B. Activated desorption at heterogeneous interfaces and long-time kinetics of hydrocarbon recovery from nanoporous media. *Nature Communications* **2016**, *7*, 11890.

(21) Feng, F.; Akkutlu, I. Y. A Simple Molecular Kerogen Pore-Network Model for Transport Simulation in Condensed Phase Digital Source-Rock Physics. *Transport in Porous Media* **2019**, *126*, 295–315.

(22) Takbiri, A.; Fathi, E.; Kazemi, M.; Belyadi, F. An integrated multiscale model for gas storage and transport in shale reservoirs. *Fuel* **2018**, *237*, 1228–1243.

(23) Gogotsi, Y.; Libera, J. A.; Güvenç-Yazicioglu, A.; Megaridis, C. M. In situ multiphase fluid experiments in hydrothermal carbon nanotubes. *Applied Physics Letters* **2001**, *79*, 1021–1023.

(24) Megaridis, C. M.; Yazicioglu, A. G.; Libera, J. A.; Gogotsi, Y. Attoliter fluid experiments in individual closed-end carbon nanotubes: Liquid film and fluid interface dynamics. *Physics of Fluids* **2002**, *14*, L5–L8.

(25) Ruthven, D. M.; Kärger, J.; Theodorou, D. N. *Diffusion in nanoporous materials*; John Wiley & Sons, 2012.

(26) Brandani, S.; Hufton, J.; Ruthven, D. Self-diffusion of propane and propylene in 5A and 13X zeolite crystals studied by the tracer ZLC method. *Zeolites* **1995**, *15*, 624–631.

(27) Falk, K.; Coasne, B.; Pellenq, R.; Ulm, F.-J.; Bocquet, L. Subcontinuum mass transport of condensed hydrocarbons in nanoporous media. *Nature communications* **2015**, *6*, 6949.

(28) Apostolopoulou, M.; Day, R.; Hull, R.; Stamatakis, M.; Striolo, A. A kinetic Monte Carlo approach to study fluid transport in pore networks. *The Journal of Chemical Physics* **2017**, *147*, 134703.

(29) Ning, Y.; Jiang, Y.; lin Liu, H.; Qin, G. Numerical modeling of slippage and adsorption effects on gas transport in shale formations using the lattice Boltzmann method. *Journal of Natural Gas Science and Engineering* **2015**, *26*, 345–355.

(30) Soulaine, C.; Creux, P.; Tchelepi, H. A. Micro-continuum Framework for Pore-Scale Multiphase Fluid Transport in Shale Formations. *Transport in Porous Media* **2018**, *127*, 85–112.

(31) Neimark, A. V.; Vishnyakov, A. Phase Transitions and Criticality in Small Systems: Vapor-Liquid Transition in Nanoscale Spherical Cavities. *The Journal of Physical Chemistry B* **2006**, *110*, 9403–9412.

(32) Firouzi, M.; Wilcox, J. Molecular modeling of carbon dioxide transport and storage

in porous carbon-based materials. *Microporous and Mesoporous Materials* **2012**, *158*, 195–203.

(33) Striolo, A.; Gubbins, K. E.; Gruszkiewicz, M. S.; Cole, D. R.; Simonson, J. M.; Chialvo, A. A.; Cummings, P. T.; Burchell, T. D.; More, K. L. Effect of Temperature on the Adsorption of Water in Porous Carbons. *Langmuir* **2005**, *21*, 9457–9467.

(34) Wang, J.; Kang, Q.; Chen, L.; Rahman, S. S. Pore-scale lattice Boltzmann simulation of micro-gaseous flow considering surface diffusion effect. *International Journal of Coal Geology* **2017**, *169*, 62–73.

(35) Mehmani, A.; Prodanović, M.; Javadpour, F. Multiscale, Multiphysics Network Modeling of Shale Matrix Gas Flows. *Transport in Porous Media* **2013**, *99*, 377–390.

(36) Clarkson, C. R.; Nobakht, M.; Kaviani, D.; Ertekin, T. Production analysis of tight-gas and shale-gas reservoirs using the dynamic-slippage concept. *SPE Journal* **2012**, *17*, 230–242.

(37) Firouzi, M.; Wilcox, J. Slippage and viscosity predictions in carbon micropores and their influence on CO2 and CH4 transport. *The Journal of Chemical Physics* **2013**, *138*, 064705.

(38) Sinha, S.; Braun, E.; Determan, M.; Passey, Q.; Leonardi, S.; Boros, J.; Wood III, A.; Zirkle, T.; Kudva, R. Steady-state permeability measurements on intact shale samples at reservoir conditions-effect of stress, temperature, pressure, and type of gas. *SPE Middle East Oil and Gas Show and Conference* **2013**, 956–970.

(39) Ortiz-Young, D.; Chiu, H.-C.; Kim, S.; Voïtchovsky, K.; Riedo, E. The interplay between apparent viscosity and wettability in nanoconfined water. *Nature Communications* **2013**, *4*.

(40) Collell, J.; Ungerer, P.; Galliero, G.; Yiannourakou, M.; Montel, F.; Pujol, M. Molecular Simulation of Bulk Organic Matter in Type II Shales in the Middle of the Oil Formation Window. *Energy & Fuels* **2014**, *28(12)*, 7457–7466.

(41) Bousige, C.; Ghimbeu, C. M.; Vix-Guterl, C.; Pomerantz, A. E.; Suleimenova, A.; Vaughan, G.; Garbarino, G.; Feygenson, M.; Wildgruber, C.; Ulm, F.-J.; *et al.*, Realistic molecular model of kerogen's nanostructure. *Nature Materials* **2016**, *15*, 576–582.

(42) Atmani, L.; Bichara, C.; J.-M. Pellenq, R.; Damme, H. V.; Duin, A. C. T. v.; Raza, Z.; A. Truflandier, L.; Obliger, A.; G. Kralert, P.; J. Ulm, F.; Leyssale, J.-M. From cellulose to kerogen: molecular simulation of a geological process. *Chemical Science* **2017**, *8*, 8325–8335.

(43) Vasileiadis, M.; Peristeras, L. D.; Papavasileiou, K. D.; Economou, I. G. Modeling of bulk kerogen porosity: Methods for control and characterization. *Energy & Fuels* **2017**, *31*, 6004–6018.

(44) Obliger, A.; Valdenaire, P.-L.; Capit, N.; Ulm, F. J.; Pellenq, R. J.-M.; Leyssale, J.-M. Poroelasticity of Methane-Loaded Mature and Immature Kerogen from Molecular Simulations. *Langmuir* **2018**, *34*, 13766–13780.

(45) Collell, J.; Galliero, G.; Vermorel, R.; Ungerer, P.; Yiannourakou, M.; Montel, F.; Pujol, M. Transport of Multicomponent Hydrocarbon Mixtures in Shales Organic Matter by Molecular Simulations. *The Journal of Physical Chemistry C* **2015**, *119 (39)*, 22587–22595.

(46) Obliger, A.; Ulm, F.-J.; Pellenq, R. J.-M. Impact of Nanoporosity on Hydrocarbon Transport in Shales' Organic Matter. *Nano Letters* **2018**, *18*, 832 – 837.

(47) Obliger, A.; Pellenq, R.; Ulm, F.-J.; Coasne, B. Free Volume Theory of Hydrocarbon Mixture Transport in Nanoporous Materials. *The Journal of Physical Chemistry Letters* **2016**, *7*, 3712–3717.

(48) Vasileiadis, M.; Peristeras, L. D.; Papavasileiou, K. D.; Economou, I. G. Transport properties of shale gas in relation to kerogen porosity. *The Journal of Physical Chemistry C* **2018**, *122*, 6166–6177.

(49) Ho, T. A.; Wang, Y.; Criscenti, L. J. Chemo-mechanical coupling in kerogen gas adsorption/desorption. *Physical Chemistry Chemical Physics* **2018**, *20*, 12390–12395.

(50) Obliger, A.; Valdenaire, P.-L.; Ulm, F.-J.; Pellenq, R. J.-M.; Leyssale, J.-M. Methane Diffusion in a Flexible Kerogen Matrix. *The Journal of Physical Chemistry B* **2019**, *123*, 5635–5640.

(51) Tesson, S.; Firoozabadi, A. Deformation and Swelling of Kerogen Matrix in Light Hydrocarbons and Carbon Dioxide. *The Journal of Physical Chemistry C* **2019**, *123*, 29173–29183.

(52) Wu, T.; Firoozabadi, A. Effect of Microstructural Flexibility on Methane Flow in Kerogen Matrix by Molecular Dynamics Simulations. *The Journal of Physical Chemistry C* **2019**, *123*, 10874–10880.

(53) Wang, Z.; Li, Y.; Liu, H.; Zeng, F.; Guo, P.; Jiang, W. Study on the Adsorption, Diffusion and Permeation Selectivity of Shale Gas in Organics. *Energies* **2017**, *10*, 142.

(54) Yu, K. B.; Bowers, G. M.; Loganathan, N.; Kalinichev, A. G.; Yazaydin, A. O. Diffusion Behavior of Methane in 3D Kerogen Models. *Energy & Fuels* **2021**, *35*, 16515–16526.

(55) Fujita, H. Free volume interpretation of the polymer effect on solvent dynamics. *Macromolecules* **1993**, *26*, 643–646.

(56) Fujita, H. Notes on Free Volume Theories. *Polymer Journal* **1991**, *23*, 1499–1506.

(57) Höhnerbach, M.; Bientinesi, P. Accelerating AIREBO: Navigating the Journey from Legacy to High-Performance Code. *Journal of Computational Chemistry* **2019**, *40*, 1471–1482.

(58) Martyna, G. J.; Tuckerman, M. E.; Tobias, D. J.; Klein, M. L. Explicit reversible integrators for extended systems dynamics. *Molecular Physics* **1996**, *87*, 1117–1157.

(59) Ismail, A. F.; Khulbe, K. C.; Matsuura, T. Gas separation membranes. *Switz. Springer* **2015**, *10*, 973–978.

(60) Pathak, M.; Huang, H.; Meakin, P.; Deo, M. Molecular investigation of the interactions of carbon dioxide and methane with kerogen: Application in enhanced shale gas recovery. *Journal of Natural Gas Science and Engineering* **2018**, *51*, 1–8.

TOC Graphic